1 Science Plan

1.1 Scientific Justification

1.1.1 Old Stars in Extended Ultraviolet Disks

The size of a galaxy is a fundamental parameter in our understanding of the evolution of galaxies. In λCDM models, galactic disks are built through mergers and the accretion of small satellites, as well as through *in situ* star formation activity (e.g., Abadi et al. 2003; Governato et al. 2004). These two growth mechanisms have distinctly different predictions for the age of the associated extended stellar population.

According to the inside-out galaxy formation scenario, the outer disk should be dominated by a smoothly distributed young population of stars (Avila-Reese & Firmani 2000). In this model, outer disk stars were either formed from star formation occurring in the galaxy outskirts, or they were transported from the inner disk regions through 'radial migration' (Roškar et al. 2008). GALEX observations carried out in the ultraviolet have shown the young stellar distribution to extend well beyond the de Vaucouleurs radius R_{25} in the so-called extended ultraviolet disk or 'XUV' galaxies (Thilker et al. 2007; Gil de Paz et al. 2007; Zaritsky & Christlein 2007; Figure 1). In a study of 458 galaxies with ultraviolet, optical, and HI data, Wang et al. (2010) find that galaxies fitting the inside-out picture of disk formation are rich in HI and have bluer, more actively star-forming outer disks, consistent with recent simulations (Bush et al. 2010). In another study of 161 spirals with multi-wavelength broadband data, Muñoz-Mateos et al. (2007) detect, on average, a mildly positive rise with radius in the specific star formation rate, which they interpret as tentative support for gradual inside-out disk build-up in the majority of systems. However, for a small subset of disks they observe significantly longer disk scalelengths in the ultraviolet compared to the near-infrared, suggesting a period of substantial recent disk growth.

In contrast to inside-out disk formation scenarios, accretion models predict that the diffuse, outermost stellar distribution is largely composed of the remnants of previously accreted satellites and tidal debris from major mergers, and thus is dominated by an older stellar population that likely exhibits substructure (Robertson et al. 2004). The Keck-based work of Ibata et al. (2005) presents such a scenario for M 31: they find stars associated with that galaxy as far as 70 kpc ($1.6R_{25}$) from the nucleus, and with velocities close to those expected for circular orbits at that distance. This stellar emission shows substructure, consistent with an accretion history. Likewise, HST provides evidence for hierarchical assembly of M 31 through observations of a 10 Gyr stellar population 35 kpc from its nucleus (Brown et al. 2008).

Similarly, Thilker et al. (2005) find knots of ultraviolet emission extending out to $4R_{25}$ in M 83, a galaxy known to have substructure in its outer disk, perhaps due to a recent (1–2 Gyr ago) encounter with NGC 5253 (Rogstad et al. 1974; van den Bergh 1980). Dong et al. (2008) and Alberts et al. (2011) use GALEX and IRAC to determine the ages and stellar masses of stars in the extended ultraviolet disks of six nearby galaxies, finding typical ages of 100–200 Myr, but extending up to over a Gyr. Likewise, Gogarten et al. (2009) find long durations for the star formation history of the outer disk of M 81. Finally, in another study of extended stellar emission in local galaxies, Herbert-Fort et al. (2009) use deep LBT and GALEX imaging to probe the blue and red stellar populations in NGC 3184 out to and beyond $1.6R_{25}$. Though NGC 3184 lacks any obvious young outer disk component, in this galaxy red stellar clusters are more prominent than their blue counterparts at the largest

radii, and in fact, the red knots appear to be correlated with the outermost fringes of the HI emission at $1.7R_{25}$.

The local extended ultraviolet disk fraction has been estimated to be ∼30% (Thilker et al. 2007; see also Zaritsky & Christlein 2007). Thilker et al. (2007) separate the XUV galaxies into two classes. Type 1 disks frequently contain filamentary, outer disk substructure, perhaps indicative of an accretion history or interaction-driven evolution, whereas Type 2 XUV galaxies exhibit an ultraviolet profile smoothly extending from the interior to the outer disk regions. Interestingly, Thilker et al. find a 2-to-1 ratio of Type 1 to Type 2 XUV disks.

Pohlen & Trujillo (2006) study a sample of 90 nearby galaxies at $g\prime$ and $r\prime$ wavelengths and find that only 10% show a smooth exponential decline to the edge of their disks; the remaining 90% show double exponential profiles. Two-thirds of the latter subset show steeper declines in the outer regions ('downbending') while one-third exhibit shallower outer profiles ('upbending'). In other words, 30% of the galaxies in the Pohlen & Trujillo study show an increasing surface brightness of optical stellar emission in the outer disks, and 30% of the galaxies studied by Thilker et al. (2007) show extended ultraviolet emission.

1.1.2 Hα in Galaxy Peripheries and Other Low Surface Brightness Regions

Star formation has long been thought to occur only above a certain threshold in gas density (e.g., Schmidt 1959; Kennicutt 1998; Leroy et al. 2008; Krumholz, McKee, & Tumlinson 2009; Bush et al. 2010). Like most other tracers of the interstellar medium, the neutral and molecular gas surface brightness profiles decrease at large galacto-centric radii (e.g., Regan et al. 2006), and thus it is not surprising that Hα surface brightness profiles typically show a sharp truncation near the R_{25} optical edge of galaxies (e.g., Martin & Kennicutt 2001; Elmegreen & Hunter 2006). However, spurred in part by the discovery of XUV disks, sensitive Hα observations in the outer disks of galaxies have shown a more complicated situation, with some Hα profiles extending to 1.5–$2R_{25}$ (Ferguson et al. 1998; Christlein, Zaritsky, & Bland-Hawthorn 2010; Goddard, Kennicutt, & Ryan-Weber 2010). The existence of pockets of star formation in the outer disks of galaxies has important implications for how galaxies grow in environments of low metallicity, low gas surface density, relatively high shear, and high HI-to-H_2 ratios (see Bigiel et al. 2010).

An intriguing recent result stems from an Hα and ultraviolet study of a sample of nearby galaxies containing a large fraction of dwarfs. At very low star formation activity levels, down to rates of $\sim 10^{-4}\ M_\odot\ \mathrm{yr}^{-1}$ that are comparable to the environments in the outer disks of normal galaxies, Lee et al. (2009) find that Hα systematically underestimates the star formation rate relative to the far-ultraviolet (see also Meurer et al. 2009). This finding is not a result of extinction, since the far-ultraviolet continuum is more impacted than Hα by dust attenuation. Moreover, the discrepancy in these star formation rate indicators is shown by Lee et al. to unlikely be due to stellar evolutionary model uncertainties, metallicity, bursty star formation histories, ionizing photon leakage, or stochasticity in the formation of high-mass stars. The most compelling alternative is a steeper initial mass function for regions of low star formation activity such as in dwarf/low surface brightness galaxies, resulting in a deficit of high-mass stars, a scenario supported by theoretical predictions (Kroupa & Weidner 2003; Weidner & Kroupa 2005, 2006; Pflamm-Altenburg et al. 2007, 2009). However, in contrast to this picture, comparisons of far-ultraviolet, near-ultraviolet, and Hα data in the outer disks of nearby galaxies point to stochasticity in high-mass star formation as the culprit for differences between Hα- and ultraviolet-based star formation rates in outer

disks, and provide no evidence for an IMF that is unique to such peripheral environments (e.g., Goddard, Kennicutt, & Ryan-Weber 2010; Alberts et al. 2011).

1.1.3 Science Questions and Goals

All of these results demonstrate a complex variety of morphologies at different wavelengths in the outer disk environment. Does the Type 1 to Type 2 ratio in XUV disks reflect the ratio of accretion-to-inside-out formation scenarios? As the inside-out disk formation theory might suggest, are Type 2 XUV galaxies also 'XHα' galaxies showing a smooth distribution of recent star formation in the outer disk regions? Likewise, according to the scenario whereby galaxies grow by accreting older stars from satellites and tidal debris, are Type 1 XUV galaxies also 'XIR' galaxies showing extended near-infrared emission that is perhaps clumpy? To be more specific, stellar ages can help to address the question of disk formation, and the Hα equivalent widths along with the IR$-$UV and FUV$-$NUV colors can be utilized to determine the ages of the outer disk stellar populations. Combined with the morphology of the stellar emission in the outer disks, such information can help to confirm or reject formation by accretion or formation via an inside-out process.

Another interesting question is related to what is seen for the galaxies with the smallest star formation rates—does the Hα-based SFR in the outer disks underestimate the ultraviolet-based star formation rate and what would the resulting implications be for the initial mass function in those environments? Additional questions are related to the radial profiles and the existence of any breaks. Is there a characteristic mass surface density and/or profile inflection for XUV disks, which could provide a unique method for detecting ultraviolet-dormant extended galaxies? How do the radial profiles compare at the three different wavelengths—are there any discernible trends in the break radius as a function of stellar population age?

We propose to obtain very deep 3.6 and 4.5 μm imaging of a sample of nearby galaxies, with two primary goals: constraining the age range of ultraviolet-bright knots of star formation in the outer disks, and quantifying how far out the evolved stellar population can be detected, yielding its mass surface density and crucial insights into the fossil record in galaxy peripheries. The combination of GALEX and IRAC data will provide a unique leverage for determining ages almost independently of IMF variations (Alberts et al. 2011), while the Hα will trace the ionizing photons of the most massive (and youngest) stars. Dust attenuation will be minimized in the outer disk regions where the dust surface density is low (see also § 1.2.4).

1.1.4 Why *Spitzer*?

The apparent size of a galaxy depends on the emission mechanism in question (stellar light, synchrotron radiation, thermal emission from dust, etc.), along with the sensitivity of the measurement. One of our goals is to simply compare the full extent of the stellar disk traced by old stars to that traced by young stars, but observations of the faint outer disk are technically challenging at any wavelength (see, e.g., de Jong 2008), particularly in the near-infrared. Fortunately, observations with *Spitzer* will provide a unique opportunity to explore the full extent of the stellar distribution with deep wide-field infrared imaging. Such observations are impossible to attempt from ground-based observatories due to the systematic and technical difficulties produced by generally variable sky levels and instruments with

small areal coverage. Furthermore, comparable ground-based optical imaging is biased toward younger, star-forming disks and thus requires significantly longer integration times to achieve similar sensitivity to stellar mass; for instance, to image an old stellar population, R band imaging on a 4-m class telescope requires $\sim$50 times the integration time to achieve a similar depth as our *Spitzer* 3.6 μm imaging. Figure 2 displays the ultraviolet, optical, and near-infrared surface brightness profiles and the stellar mass surface density profiles for the XUV galaxy NGC 5474, along with a Cycle 6 example that meets our desired sensitivity. Even if outer stellar disks could be detected in the optical, conversion from observed optical surface brightness to stellar mass density is highly dependent on the assumed stellar population age, initial mass function, and metallicity. Thus, observations with *Spitzer* is the only possible approach that will allow us to trace the stellar distribution to unprecedented levels at wavelengths that are insensitive to dust extinction and the galaxy's star formation.

1.2 Technical Plan

1.2.1 Sample Definition

Our sample of XUV galaxies originates from the comprehensive GALEX Ultraviolet Atlas of Nearby Galaxies (Gil de Paz et al. 2007). Galaxies with ultraviolet emission significantly beyond the R_{25} radius were identified via ultraviolet surface brightness profiles. Gil de Paz and collaborators have undertaken a comprehensive ground-based campaign at Calar Alto to follow-up these XUV targets with deep broadband and Hα imaging. Focusing on XUV galaxies with deep ancillary data allows for a detailed comparison of the spatially extended stellar populations spanning a wide range of ages. We have taken this subsample of the GALEX Atlas and further selected only moderate-size ($D_{25} < 5.5'$), high Galactic latitude galaxies ($|b| > 35°$) within 20 Mpc that lack nearby companions, leaving us with a total of 12 XUV galaxies. Excluding galaxies at low Galactic latitudes minimizes contamination by foreground stars, and selecting only those with major optical diameters smaller than $5.5'$ avoids excessively long AORs. Adding a distance cut ensures reasonable spatial resolution—a $7''$ surface brightness profile bin width, for example, corresponds to 0.3 kpc at 10 Mpc. The balance between Types 1 and 2 XUV disks is similar to that found in the larger galaxy population found by Thilker et al. (2007).

To enable a fair interpretation of the XUV galaxies, we have selected a control sample of non-XUV galaxies for which we also have access to deep GALEX ultraviolet and ground-based broadband and Hα imaging. The control sample is taken from the SINGS sample of nearby galaxies (Kennicutt et al. 2003; Dale et al. 2007), following the same selection criteria of $|b| > 35°$, $D_{25} < 5.5'$, and $D < 20$ Mpc. After further excluding SINGS galaxies lacking GALEX FUV and NUV imaging and those that appear to be interacting with nearby neighbors, we are left with a control sample of six non-XUV SINGS galaxies where the ultraviolet emission is comparable in extent to that at optical wavelengths (Figure 3). The control sample includes a similar range of morphologies and optical sizes as those found in the XUV sample; issues such as foreground/background contamination and flat-fielding will be similar for the primary and control samples. As this project requires deep imaging with well-defined sky levels, we used SPOT to determine the typical infrared sky level for each target at both 3.6 and 4.5 μm. In all cases, the expected infrared sky levels are low, less than 100 kJy sr^{-1}. Taken as a whole, our survey of very deep 3.6 μm imaging will allow us to compare the extent and nature of the diffuse stellar distributions in galaxies exhibiting a wide variety of physical characteristics.

1.2.2 Observing Plan

We have analyzed the ultraviolet surface brightness profiles of our 12 XUV galaxies. The average $R_{\rm UV}/R_{25}$ ratio for our XUV targets is 2.9. In terms of the 3.6 μm extent, analysis of our deep Cycle 6 data on HI extended galaxies shows some 3.6 μm surface brightness profiles extend beyond $3-4R_{25}$. Our proposed 3.6 μm observations are thus designed to map at least to $5R_{25}$ (Figure 4). This will ensure enough coverage to adequately sample any extended stellar distributions while still allowing ample area for determining the sky value.

AORs are constructed using the successful strategy utilized for our Cycle 6 program. Mosaics are built upon a grid of 100″ spacings (∼one-third the IRAC field of view). Two sets of maps will be obtained for each source to enable asteroid removal and data redundancy, and to build up the map sensitivity to the desired level. Thus, at any given location within the map cores there will be a total of 18 × 100 s frames resulting in a net integration per sky position of 1800 s (along with a 1200 s ∼100″-wide "inner periphery" and a 600 s ∼100″-wide "outer periphery"). The smallest maps will be 8x8 mosaics, ensuring at least 10′ map cores at the deepest 1800 s effective integration. We will center the mosaics for 3.6 μm observations, but even our smallest maps have sufficient sky coverage that the field of view of the corresponding 4.5 μm mosaic will include the galaxy as well.

Our sample is restricted to galaxies with low infrared sky levels (less than 100 kJy sr^{-1} at 3.6 μm), and thus we expect to achieve a 1σ noise level per pixel of 0.0018 MJy sr^{-1} at 3.6 μm (based on our Cycle 6 data and on SENS-PET predictions). Further, the simultaneous images at 4.5 μm will have a per pixel surface brightness sensitivity of 0.0027 MJy sr^{-1}; while the 4.5 μm mosaic will not be centered on the galaxy, it will provide both an independent observation of the extended stellar distribution and provide the potential to trace the faint stellar population to even larger radii (along the axis of observation).

These deep mosaics will allow us to trace the stellar distribution to unprecedented levels of a few × 0.01 $M_\odot$ pc^{-2}, at wavelengths that are relatively insensitive to dust and the galaxy's past star formation history. Indeed, the 1800 s integration per position on the sky represents a much deeper effort than other surveys of nearby galaxies, e.g., SINGS ($N_{\rm gal}=75; T=240$ s; Kennicutt et al. 2003), LVL ($N_{\rm gal}=258; T=240$ s; Dale et al. 2009), S^{4}G ($N_{\rm gal}\sim 2300; T=240$ s; Sheth et al. 2010), and the IRAC GTO project ($N_{\rm gal}=100; T=60$ or 150 s; Pahre et al. 2004). These surveys reach a 1σ sensitivity of a few to several kJy sr^{-1}, which is typically at the 5% level with respect to the near-infrared surface brightness (Regan et al. 2006). With (7″) azimuthal averaging, our proposed observations will go to 0.2 kJy sr^{-1}, a necessity for obtaining high signal-to-noise in the faint outer disks beyond R_{25}. For comparison, WISE achieves a 3.4 μm sensitivity larger than 1 kJy sr^{-1} over a 5′ × 5′ area (Wright et al. 2010).

1.2.3 Data Processing

The post-pipeline processing of the data should be straightforward, given our substantial experience with SINGS, LVL, and Cycle 6 programs. The multi-epoch, multiple-pointing observations for each galaxy will be combined into a single mosaic for each band using the MOPEX mosaicking software. Additional post-BCD processing will include distortion corrections, rotation of the individual frames, bias structure and bias drift corrections, image offset determinations via pointing refinements from the SSC pipeline, detector artifact removal, constant-level sky subtraction, and image resampling to 0.75″ pixels using drizzling techniques. The drizzling slightly improves the final PSF over the native one.

The two largest challenges to measuring stellar emission in the extreme outer disks are the presence of foreground stars/background galaxies and the stability of the sky levels within the large maps. As explained above, we plan to minimize the first issue by constraining our sample to $|b| > 35°$. Furthermore, we have extensively explored how best to mask foreground stars and background galaxies. The optimal approach that we have converged upon relies on a two-pronged strategy. First, we identify foreground stars and background point sources using IRAF/DAOPhot. Second, we rely on SExtractor (Bertin & Arnouts 1996) to identify extended background galaxies. Empirical checks will be made via comparison with the Hα, ultraviolet, and broadband optical imaging. Next, foreground and background objects are masked using an IDL script that utilizes the SExtractor ellipses for the extended targets and the SSC-provided IRAC 2D PSFs for the foreground stars and point sources.

To assess the sky stability, we have analyzed maps from our Cycle 6 program that is being executed at the same imaging depth. Inspection of our mosaics, which span scales as large as $\sim 1°$, shows sky variations less than 0.001 MJy sr^{-1}. We will map the entire field of view during each AOR (two per target), and thus changes across the field due to variations in zodiacal light will be minimized. In short, we have adopted our Cycle 6 mapping strategy for this proposal, and that strategy has proven successful for a similar set of goals.

1.2.4 Data Analysis

An important parameter in deriving accurate surface brightness profiles is the sky value for each field. We will employ a curve of growth analysis to constrain sky levels in azimuthally averaged data. Once the sky level has been determined, azimuthal averages will allow us to probe surface brightness levels well below the single pixel detection limits (Figure 2). We will examine the surface brightness profiles at 3.6 and 4.5 μm to look for evidence of disk truncation, as well as to examine the extent of the faint stellar distribution relative to the ultraviolet, optical, and Hα emission. Stellar masses will be computed using the 3.6 and 4.5 μm data, and star formation histories will be calculated based on the entire multi-wavelength dataset (e.g., Panter et al. 2007). The presence of 3.3 μm PAH emission in the IRAC1 band will likely be minimal due to the negligible dust present in outer disks (Gil de Paz et al. 2007a; Dong et al. 2008). Supporting this view is the low metallicity nature of outer disk regions ($Z/Z_{\odot} = 1/5 - 1/10$; Gil de Paz 2007b; Goddard et al. 2010b), coupled with the fact that low metallicity is known to depress PAH emission (e.g., Engelbracht et al. 2008). Indeed, a small IRAC study of outer disk regions in five spiral galaxies, employing a single pointing in each galaxy at $\sim 2R_{25}$ with an imaging depth similar to that proposed here, shows no evidence of PAH emission (Alberts et al. 2011).

1.2.5 Management Plan

PI Dale will coordinate the scientific efforts and management of the project and serve as Technical Contact. Data processing, including mosaicking and curve of growth analysis, will be led by Staudaher, who has extensive experience from our Cycle 6 projects described in § 3. All team members will participate in the analysis of the data. Gil de Paz and Thilker will provide expertise for the ultraviolet data, including post-pipeline-processed images and surface brightness profiles. Gil de Paz will also contribute analysis of his deep Hα and optical broadband imaging for the sample. van Zee and Barnes will lead on comparisons to the available HI data. Calzetti will provide expertise on using multi-wavelength data to investigate the ages and characteristics of the stellar populations of the outer disks.

1.3 Figures, Tables & References

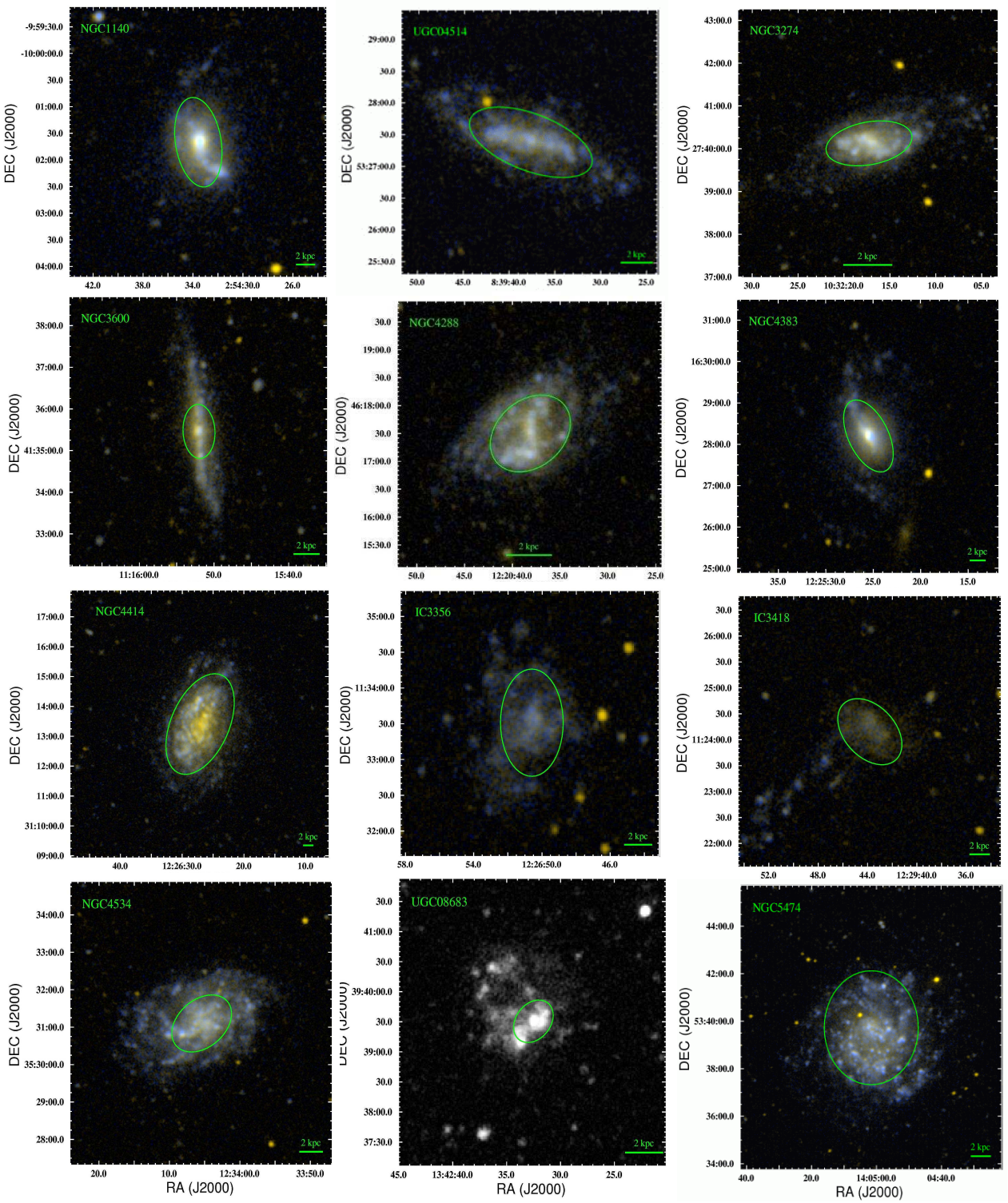

Figure 1: FUV-NUV false-color images for the XUV galaxies in the sample. The ultraviolet emission extends well beyond the optical extent indicated by the $D_{25} \times d_{25}$ ellipses.

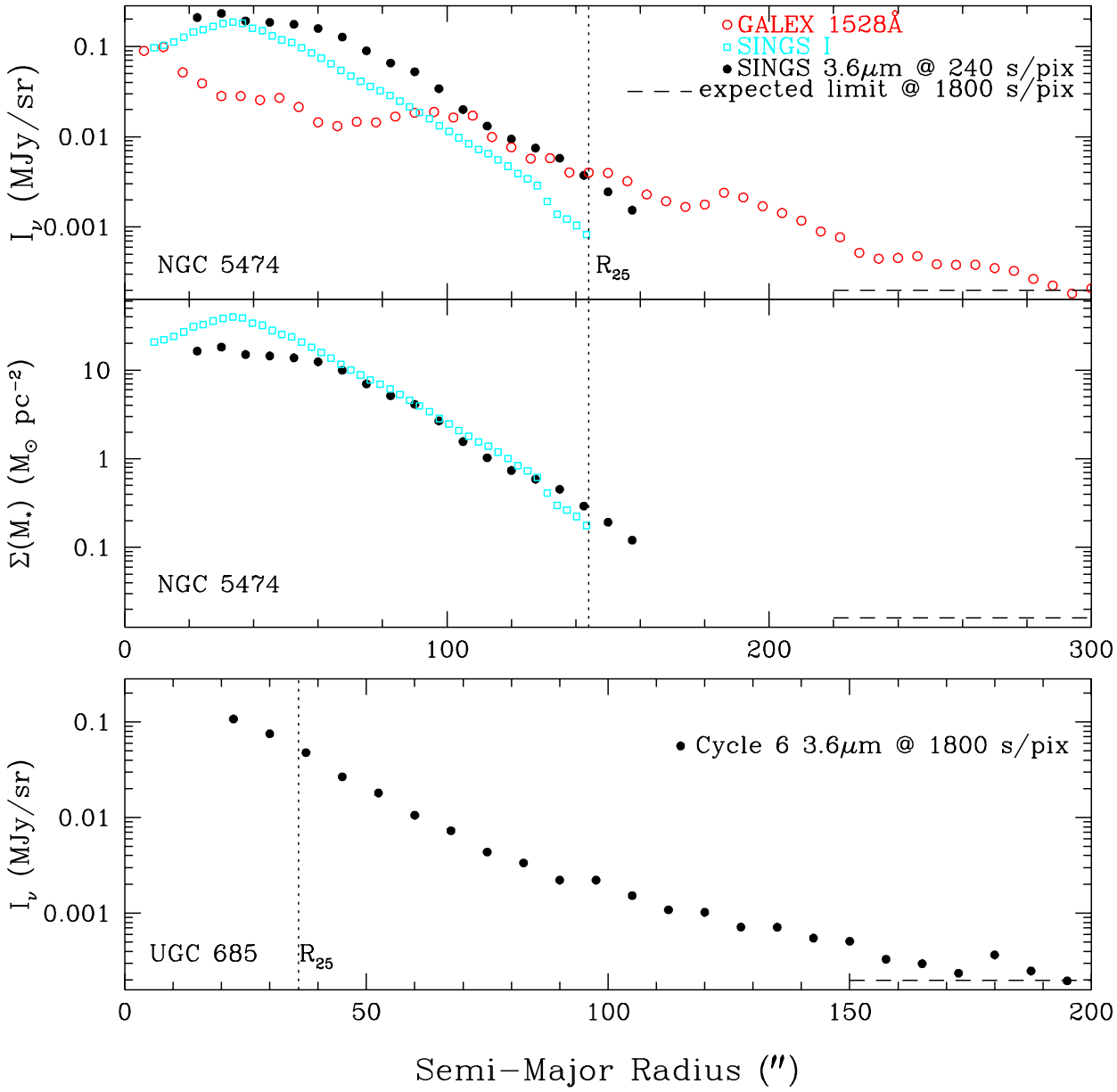

Figure 2: **Top**: The ultraviolet, optical, and near-infrared surface brightness profiles for XUV galaxy NGC 5474. The UV profile, shown with open red circles, extends far beyond R_{25}. The currently-available 3.6 μm surface brightness profile, shown with filled black circles, is at the relatively shallow depth provided by the SINGS survey (Dale et al. 2007). The predicted surface brightness limit for our survey is indicated by the dashed line. This expectation is based on SENS-PET predictions and is consistent with the analysis of our Cycle 6 program data at the same imaging depth of 1800 s/pix (see bottom panel). **Middle**: The stellar mass surface density profiles based on the 3.6 μm and I band SINGS data, assuming $M/L \sim 2-3 M_{\odot}/L_{\odot}$ for a galaxy at 10 Mpc. The expected sensitivity to stellar mass with our proposed observations goes well below that available from extant data. **Bottom**: The near-infrared surface brightness profile for UGC 685 from our Cycle 6 program to deeply image HI-extended galaxies. These azimuthally-averaged data, taken at the same 1800 s/pix integration as that planned in this proposal, reach our targeted 3.6 μm sensitivity of ~ 0.2 kJy/sr.

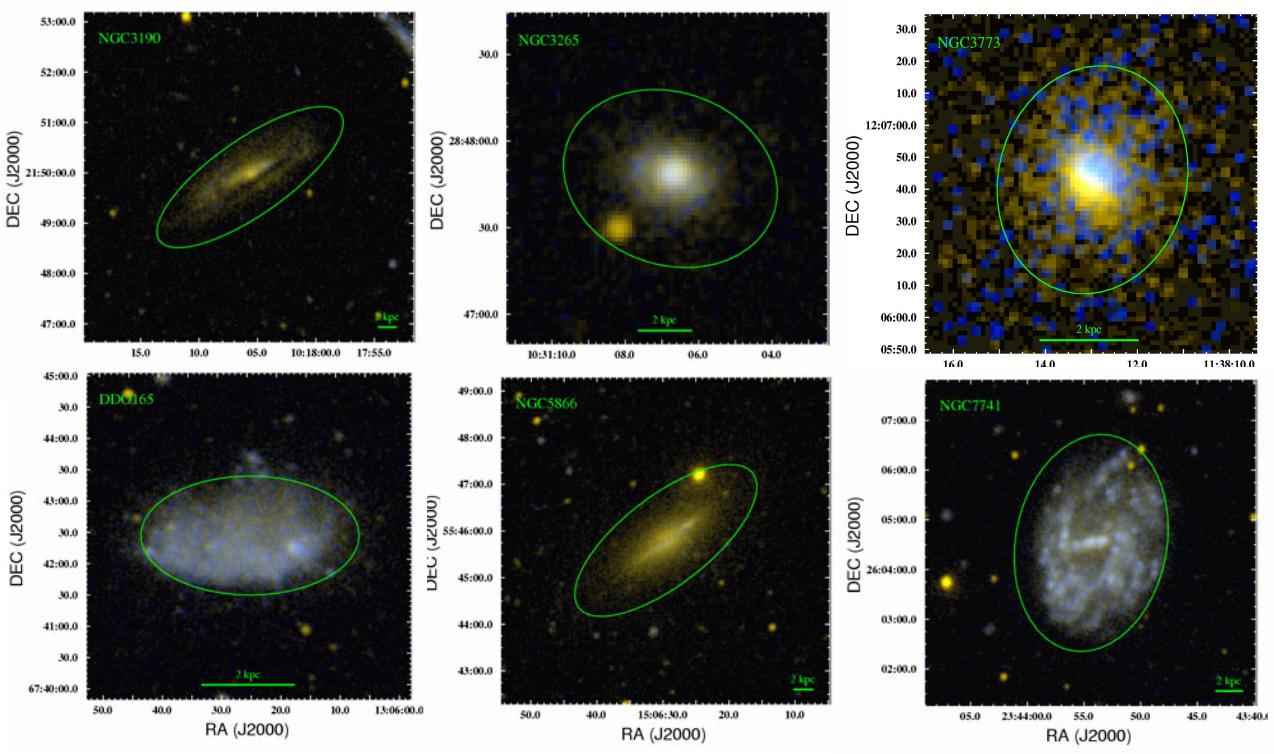

Figure 3: FUV-NUV false-color images for the control sample of non-XUV galaxies. The ellipses again are sized according to $D_{25} \times d_{25}$.

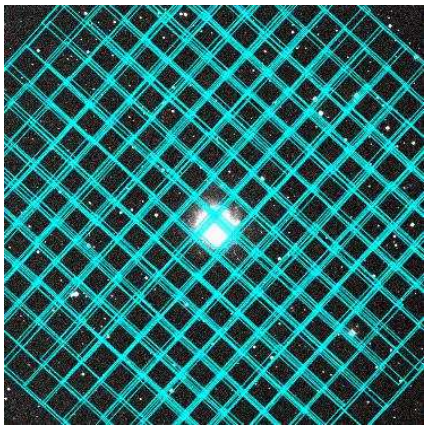

Figure 4: An example IRAC AOR footprint, overlaid on a $25' \times 25'$ DSS image of NGC 5474. The mosaic "core" of $23.3'$ is ~ 5 times the $4.8'$ D_{25} diameter for this galaxy (see § 1.2.2).

References

Abadi, M.G., Navarro, J.F., & Steinmetz, M. 2006, MNRAS, 365, 747
Alberts, S. et al. 2011, in press
Avila-Reese, V. & Firmani, C. 2000, RMxAA, 36, 23
Bertin, E. & Arnouts, S. 1996, A&AS, 117, 393
Brown, T.M., et al. 2008, ApJ, 685, L121
Bush, S.J., Hayward, C.C., Thilker, D., Hernquist, L., & Gurtina, B. 2010, ApJ, 713, 780
Christlein, D., Zaritsky, D., & Bland-Hawthorn, J. 2010, MNRAS, 405, 2549
Dale, D.A. et al. 2007, ApJ, 655, 863
Dale, D.A. et al. 2009, ApJ, 703, 517
de Jong, R.S. 2008, MNRAS, 388, 1521
Dong, H., Calzetti, D., Regan, M., Thilker, D., Bianchi, L., Meurer, G.R., & Walter, F. 2008, AJ, 136, 479
Elmegreen, B. & Hunter, D. 2006, ApJ, 636, 712
Engelbracht, C. et al. 2008, ApJ, 678, 804
Ferguson, A., Wyse, R., Gallagher, J., & Hunter, D. 1998, ApJL, 506, L19
Gil de Paz, A. et al. 2007a, ApJS, 173, 185
Gil de Paz, A. et al. 2007b, ApJ, 662, 115
Goddard, Q.E., Kennicutt, R.C., & Ryan-Weber, E.V. 2010, MNRAS, 405, 2791
Goddard, Q.E., Bresolin, F., Kennicutt, R.C., Ryan-Weber, E.V. et al. 2010, MNRAS, in press
Gogarten, S.M., et al. 2009, ApJ, 691, 115
Governato, F. et al. 2004, ApJ, 607, 688
Herbert-Fort, S. et al. 2009, ApJ, 700, 1977
Ibata, R., Chapman, S., Ferguson, A.M.N., Lewis, G., Irwin, M., & Tanvir, N. 2005, ApJ, 634, 287
Kennicutt, R.C. 1998, ARAA, 36, 189
Kennicutt, R.C. et al. 2003, PASP, 115, 928
Kroupa, P. & Weidner, C. 2003, ApJ, 598, 1076
Krumholz, M.R., McKee, C.F., & Tumlinson, J. 2009, ApJ, 699, 850
Lee, J.C. et al. 2009, ApJ, 706, 599
Leroy, A.K., Walter, F., Brinks, E., Bigiel, F., de Blok, W.J.G., Madore, B. et al. 2008, AJ, 136, 2782
Martin, C.L. & Kennicutt, R.C. 2001, ApJ, 555, 301
Meurer, G.R. et al. 2009, ApJ, 695, 765
Pahre, M.A., Ashby, M.L.N., Fazio, G.G., & Willner, S.P. 2005, ApJS, 154, 235
Panter, B., Jimenez, R., Heavens, A.F., & Charlot, S. 2007, MNRAS, 378, 1550
Pflamm-Altenburg, J., Weidner, C., & Kroupa, P. 2009, MNRAS, 395, 394
Pohlen, M. & Trujillo, I. 2006, 454, 759
Regan, M. et al. 2006, ApJ, 652, 1112
Robertson, B., Yoshida, N., Springel, V., & Hernquist, L. 2004, ApJ, 606, 32
Rogstad, D.H., Lockart, I.A, & Wright, M.C.H. 1974, ApJ, 193, 309
Roškar, R., Debattista, V.P., Stinson, G.S., Quinn, T.R., Kaufmann, T., Wadsley, J. 2008 ApJL, 684, L79
Schmidt, M. 1959, ApJ, 129, 243
Thilker, D.A. et al. 2005, ApJL, 619, L79
Thilker, D.A. et al. 2007, ApJS, 173, 538
van den Bergh, S. 1980, PASP, 92, 122
Weidner, C. & Kroupa, P. 2005, ApJ, 625, 754
Weidner, C. & Kroupa, P. 2007, MNRAS, 365, 1333
Wright, E. et al. 2010, AJ, 140, 1882
Zaritsky, D. & Christlein, D. 2007, AJ, 134, 135

2 Brief Team Resume

Daniel A. Dale (Wyoming) is an expert on studies of star formation from low- to intermediate-redshift, as well as on the infrared spectra and panchromatic broadband spectral energy distributions of normal galaxies. He has extensive experience with *Spitzer* observations and data processing, as a CoI on SINGS, as a CoI on the Cycle 4 Local Volume Legacy Project (LVL), and as a CoI on the two Cycle 6 projects described in the next section.
Kate L. Barnes (Indiana) is an astronomy graduate student. Her Ph.D. dissertation examines star formation rate indicators in the outer edges of spiral galaxies. She is PI on a Cycle 6 study of the extended disk in M 83.
Daniela Calzetti (UMass) is an expert on multi-wavelength observations of star formation activity in nearby galaxies. She is a member of the SINGS, LVL, among other related *Spitzer* programs.
Armando Gil de Paz (UC Madrid) is an expert on the multi-wavelength emission from normal galaxies and blue compact dwarf galaxies. He is a member of the SINGS and LVL legacy teams, and is a leading expert on GALEX observations of galaxies, including those with extended ultraviolet emission.
Shawn M. Staudaher (Wyoming) is a first-year graduate student. He spent the previous two years as a post-baccalaureate research assistant with Dale. He has led the IRAC data processing and mosaic construction for the two Cycle 6 programs described in the following section.
David Thilker (Johns Hopkins) is an expert on the multi-wavelength properties of nearby galaxies. His discovery of extended ultraviolet emission in M 83 has led to intense efforts to understand star formation in galaxy peripheries.
Liese van Zee (Indiana) is an expert on galaxy formation and evolution with an emphasis on investigating the links between star formation, elemental enrichment, and gas distribution and kinematics in star-forming galaxies. She has extensive experience working with multi-wavelength data sets (UV, optical, IR, and radio). She is PI of a Cycle 6 program on HI extended disks described in the following section, and is CoI on LVL.

Selected Related Publications

The Calibration of Far-Infrared Monochromatic Star Formation Rate Indicators
Calzetti et al. 2010, ApJ, 714, 1256
An Ultraviolet-to-Radio Broadband Spectral Atlas of Nearby Galaxies
Dale et al. 2007, ApJ, 655, 863
The *Spitzer* Local Volume Legacy: Survey Description and Infrared Photometry
Dale et al. 2009, ApJ, 703, 517
The GALEX Ultraviolet Atlas of Nearby Galaxies
Gil de Paz et al. 2007, ApJS, 173, 185
A Search for Extended Ultraviolet Disk (XUV-Disk) Galaxies in the Local Universe
Thilker et al. 2007, ApJS, 173, 538
Spectroscopy of Outlying HII Regions in Spiral Galaxies: Abundances and Radial Gradients
van Zee et al. 1998, AJ, 116, 2805

3 Summary of Existing Programs

Liese van Zee is the PI of 60094, a 69.7-hour Cycle 6 Warm Mission program to probe the older stellar population in the outskirts of galaxies with extended HI disks. The observations for this program were completed in August 2010. The data have been post-pipeline processed, and we have optimized the creation of their image mosaics, developed routines for masking foreground stars and background galaxies, extracted surface brightness profiles, and compared the radial extent of the older population to the HI radius. Preliminary results are included in this proposal.

Kate Barnes is the PI of 60116, a 30.2-hour Cycle 6 Warm Mission program to probe the extended older stellar population in M 83. The data have been post-pipeline processed, and we have optimized the creation of their image mosaics, developed routines for masking foreground stars and background galaxies, extracted surface brightness profiles, and compared the radial extent of the older population to the HI radius.

Daniel Dale is Technical Contact for the above two programs. Dale is leading the data processing efforts on these two programs.

Daniela Calzetti is the PI of 20289 and 30753, Cycle 2 and 3 programs to probe the star formation and dust content in the outer parts of nearby galaxies. Results from the first program are published (Dong et al. 2008) and results from the second project are in press (Alberts et al. 2011).

4 Observation Summary Table

Galaxy	Position (J2000)	$D_{25} \times d_{25}$ (arcmin)	$D_{\rm UV}/D_{25}$	# grid points	AOR (hrs)	$f(K_{\rm s})$ (Jy)	Type
NGC1140	025433.6−100140	1.7×0.9	3.0	8x 8	4.1	0.042	XUV 2
UGC04514	083937.7+532723	2.1×0.9	2.2	8x 8	4.1		XUV 1
NGC3274	103217.3+274008	2.1×1.0	3.0	8x 8	4.1	0.036	XUV 2
NGC3600	111552.0+413527	1.3×0.8	3.6	8x 8	4.1	0.055	XUV 1
NGC4288	122038.1+461730	1.6×1.2	2.8	8x 8	4.1	0.032	XUV 1
NGC4383	122525.5+162812	1.9×1.0	3.5	8x 8	4.1	0.106	XUV 1
NGC4414	122627.1+311325	3.6×2.0	1.9	13x13	10.6	1.110	XUV 1
IC3356	122650.5+113332	1.5×0.9	2.4	8x 8	4.1		XUV 1
IC3418	122943.8+112409	1.5×1.0	2.7	8x 8	4.1		XUV 1
NGC4534	123405.4+353106	1.9×1.3	3.2	8x 8	4.1	0.150	XUV 2
UGC08683	134232.5+393930	0.8×0.6	5.3	8x 8	4.1		XUV 1.5
NGC5474	140312.5+542056	4.8×4.3	2.2	16x16	16.0	0.114	XUV 1.5
NGC3190	101805.6+214956	4.4×1.5	1.0	15x15	14.1	0.741	non-XUV
NGC3265	103106.7+284748	1.3×1.0	1.2	8x 8	4.1	0.048	non-XUV
NGC3773	113813.0+120644	1.2×1.0	1.3	8x 8	4.1	0.035	non-XUV
DDO165	130624.8+674225	3.5×1.9	1.4	13x13	10.6	0.037	non-XUV
NGC5866	150629.5+554504	4.7×1.9	1.1	16x16	16.0	1.263	non-XUV
NGC7741	234354.4+260432	4.4×3.0	1.2	15x15	14.1	0.094	non-XUV

There are 130.1 hrs total requested for this observing program.

5 Modification of the Proprietary Period

No modification to the proprietary period is requested for this program.

6 Summary of Duplicate Observations

There are no duplicate observations. Observations by the SINGS (P00159), LVL (P40204), and S^{4}G (P61060-8) programs for UGC 04514, NGC 3274, NGC 3600, NGC4288, IC 3356, NGC 4534, NGC 5474, NGC 3190, NGC 3265, NGC 3773, DDO 165, NGC 5866 do not have the depth (2×4×30 s/pix=240 s/pix) and field of view to constitute our observations as duplications. A few programs have observed a handful of other galaxies, and again our duplications are deeper and more extended to not be considered duplications: NGC 1140 (P00059), NGC 4383 (P30945), NGC 4414 (P00069), NGC 7741 (P00069), IC 3418 (P03418).

7 Summary of Scheduling Constraints/ToOs

There are no scheduling constraints or ToOs in this program.